Characterizing Carbon-Nanotube Devices for an Integrated Sensor System

by

Kyeong-Jae Lee
B.S. Computer Engineering
University of Virginia, 2005

Submitted to the Department of Electrical Engineering and Computer Science
in partial fulfillment of the requirements for the degree of

Master of Science

at the

MASSACHUSETTS INSTITUTE OF TECHNOLOGY

June 2007

Author .....
Department of Electrical Engineering and Computer Science
June 2007

Certified by .....
Jing Kong
Assistant Professor
Thesis Supervisor

Accepted by .....
Arthur C. Smith
Chairman, Department Committee on Graduate Students

Characterizing Carbon-Nanotube Devices for an Integrated Sensor System

by

Kyeong-Jae Lee

B.S. Computer Engineering

University of Virginia, 2005

Submitted to the Department of Electrical Engineering and Computer Science
on June 2007, in partial fulfillment of the
requirements for the degree of
Master of Science

Abstract

While carbon nanotubes (CNT) offer promise for future nano-electronic applications, reliably controlling CNT growth has been a big challenge. As-grown devices can have a number of different nanotubes, which can be either metallic or semiconducting and also vary in diameter. These factors affect the electrical properties, which are important in particular for chemical sensing applications. In this thesis, arrays of CNT field-effect transistors (FET) are fabricated and the resistance variation of as-grown devices is characterized. Each CNT array is exposed under varying concentrations of NO_2 as the conductance is monitored. The effects of gas adsorption on the metal contact and the CNT channel are treated separately in this work. A charge transfer and site-binding model is applied to understand the CNT-NO_2 interaction, and a Schottky-barrier modulation effect is used to describe the metal-NO_2 interaction. This model is applied to both the transient and steady-state response of the normalized conductance change for various devices. Devices of a different design are also fabricated, either by selectively exposing certain regions of a device to NO_2 or using a different metal contact. The response of such devices show the importance of gas molecules interacting with both the metal and CNT. Finally, a prototype CMOS-CNT sensor system is demonstrated. This hybrid system demonstrates the need for variation-toleration circuit interfaces and highlights some outstanding issues regarding integration for full scale CNT circuit applications.

Thesis Supervisor: Jing Kong
Title: Assistant Professor

Acknowledgments

The Sovereign Lord has given me an instructed tongue,
to know the word that sustains the weary.
He wakens me morning by morning,
wakens my ear to listen like one being taught.

Isaiah 50:4

Thank you Jesus, my Lord, my best friend. You are my everything, and without your wisdom and endless grace I would not be standing here today as I am.

I would like to thank my advisor, Professor Jing Kong for her guidance and patience. Your advice and support has made this possible. Thank you for giving me this research opportunity. I also thank Taeg Sang Cho and Professor Anantha Chandrakasan for the wonderful collaboration that has made this project meaningful. Thank you Anantha for your support and ideas. Taeg Sang, I truly owe my gratitude to you. As a collaborator, as a friend, taking a concept all the way to demonstrating a working system, this experience has been all the more satisfying. I wish you the best on your next endeavors. I am also grateful to MARCO and Intel for providing funding during the project. Thanks also to everyone who has been a part of the Nano-materials and Electronics Group -Mario, Hootan, Alfonso, Dan, Bin, Aurea, Stevie, Ervin, and Jikang- for all your support and discussions. I have learned so much from all of you.

Thank you, Ye-ryoung, Eunjee, Eun-Suk, Blume, and Renee for all your prayers and support. Ye-ryoung, every step together has been meaningful and I am grateful for you. Finally, I owe very special thanks to my family. I thank my parents, Jong-Kun Lee and Soyeon Mah, and my brother, Seong-Jae Lee for always being there for me. You all know how much this means to me. Your endless love, encouragement, and prayers have made me strong. I love you all so much.

Contents

1 Introduction **13**

2 Characterizing Sensor Array **15**

2.1 Device Fabrication 15

2.2 Device Variations 16

2.2.1 Metal-Nanotube Contact 17

2.2.2 Measurement Results 18

2.3 Sensor Array 19

2.3.1 Gas Experiment Setup 20

2.3.2 Linear Sensing Response 21

2.3.3 Gating Effects 22

3 Understanding Gas Adsorption **25**

3.1 Source of Conductance Change 25

3.1.1 Schottky Barrier Modulation Due to Gas Adsorption 26

3.1.2 Charge Transfer to Nanotube 28

3.2 Modeling Gas Adsorption 30

3.3 Application to Data 32

3.3.1 Parameter Variation 32

3.3.2 Al-contacted Devices 36

3.3.3 Partially Exposed Devices 38

3.3.4 Surface Binding 41

4 CMOS-CNT Sensor System **45**

5 Conclusions **49**

List of Figures

2-1 Schematic diagram of fabrication steps for CNTFET devices. 16

2-2 Histogram of low-bias resistance values. Part of the data was provided by Daniel Nezich. All devices were grown from a Fe/Mo-based catalyst with the same geometry (500nm oxide, 4μm channel, Cr/Au contacts). 19

2-3 Setup used for gas sensing experiments. Mass flow controllers, gas chamber, and measurement circuitry are shown 20

2-4 Schematic of the conductance measurement circuitry. A data-acquisition unit controls the bias and gate voltages of the CNT FETs, while a current-voltage converter relays the measured signal back to the PC. . 21

2-5 Resistance change upon NO_2 exposure. The response is largely linear, while large deviations exist for small R_0 values. 22

2-6 Effects of gating for exposure to NO_2 (300ppm) (a) Resistance change for various devices (b) Transient response with no gating (c) Transient response with gate voltage (5V) applied. 23

3-1 Dependence on surface binding energies. Assuming values of b=-1, δ=1, and $R_M/R_{CNT} = 1$ 33

3-2 Dependence on b and δ. Assuming default values of $E_{b.M}$=0.4eV, $E_{b.NT}$=0.4eV, b=-1, δ=1, and R_M/R_{CNT}=1 33

3-3 Resistance (Conductance) change as a function of initial resistance (conductance). Assumes a fixed R_{CNT}=50$k\Omega$ and exposure to 100 ppm NO_2. Normal conditions use values of $E_{b.M}$=0.4eV, $E_{b.NT}$=0.4eV, b=-0.5, and δ=0.5. Either b or δ is set to zero in the limiting case. . . 35

3-4 Experimental data on ΔG vs. G_0. Lines represent data fits. NO_2 fit assumes values of $E_{b.M}$=0.8eV, $E_{b.NT}$=0.43eV, b=-10, and δ=0.05. (1) Data from [21] 36
3-5 Resistance response for Al-contacted devices exposed to 300ppm NO_2. 37
3-6 Transient response to 300ppm NO_2 for (a) Cr/Au and (b) Al-contacted device. 37
3-7 Optical image of (a) contact-exposed and (b) CNT-exposed devices. . 39
3-8 Transient response of a (a) fully-exposed (b) CNT-exposed and (c) contact-exposed device upon exposure to 50ppm and 300ppm NO_2. Light-colored lines represent the experimental data and dark-colored lines represent fitted curves. 40
3-9 Transient response of contact-exposed devices, where (a) R_0=103kΩ and (b) R_0=52kΩ, exposed to 300ppm NO_2. Light-colored lines represent experimental data, and dark-colored lines are fitted curves. . . . 41
3-10 Pressure dependence of a CNT-exposed device. Lines represent fitted curves. 42
3-11 Pressure dependence of Al-contacted devices. Lines represent fitted curves. 43
3-12 Pressure dependence of (a) standard (Cr/Au, fully-exposed) devices and (b) a PEI-coated device from [32]. Lines represent fitted curves. . 43

4-1 Diagram of CMOS sensor interface. Courtesy of Taeg Sang Cho [8] . 46
4-2 Die photo of CNT sensor array. Metal pads are designed to be placed along the outer boundary, which is optimal for wire-bonding. 47
4-3 Experimental setup for CMOS-CNT system testing. CNT sensor chip is placed on a chip holder inside the gas chamber. CMOS chip placed outside of the chamber. Gas lines, power sources, and logic analyzer are not shown. Courtesy of Taeg Sang Cho 48
4-4 Measurement results from CMOS-CNT system. Two different sensor chips were exposed to NO_2 at different concentrations. 48

List of Tables

3.1 Fitting parameters for Figure 3-6 38
3.2 Fitting parameters for $\Delta G/G_0$ as a function of pressure. Curves shown in Figures 3-10, 3-11, and 3-12 42
3.3 Extracted parameters from Langmuir constants (K_M, K_{NT}) in Table 3.2 43

Chapter 1

Introduction

Chemical gas detection is used in environmental monitoring applications and many industrial processes. With the emergence of nanotechnology, new sensing materials are being developed and widespread interest is found in developing chemical sensor systems using these nano-materials. Such interest bridges across many fields of research, ranging from modifying material properties at the molecular level, to designing low-cost and reliable circuit interfaces, and even to optimizing advanced data communication schemes for wireless sensor networks. Much work remains to fully integrate nanotechnology with existing circuit platforms and establish them as a viable technology.

Among many materials, carbon nanotubes (CNT) have received much attention in recent years. CNTs are nanometer-diameter cylinders formed from rolled-up graphene sheets [14]. CNTs exhibit high conductivity and great stability, making them promising candidates for nano-electronics [2, 28, 45].

Since the initial work of Kong et al. [19] and Collins et al. [9], many research groups have investigated the use of CNTs as chemical and biological sensors [32, 36, 37, 40]. CNTs can be highly sensitive even at room temperature unlike many other sensing technologies. This feature renders a micro-hotplate unnecessary, making CNTs particularly attractive for low-power applications. CNTs also have nanometer range diameters and all the atoms exposed on the surface. This allows miniaturization and means for chemical coating to achieve high selectivity to specific chemical agents.

However, current fabrication methods generally yield CNT devices with large resistance variations, and CNT sensors tend to exhibit fast response but slow recovery time to chemical gases. Ultimately, device variations and technology integration issues must be resolved before any CNT sensor devices can become practical.

CNT sensors are typically fabricated either as thin films or as field-effect transistors (FET), and high sensitivity can be achieved through several means. Capacitance sensing of CNT thin films has proven to be effective for vapors at low pressures [39, 37]. Defects can also be introduced to form low-energy sorption sites favorable to molecule binding and charge transfer. Robinson et al. have shown that a small number of oxidized defect sites ($\sim$2% of carbon atoms) on the CNT can produce an increase in charge transfer by $\sim$1000% [34]. While individual semiconducting nanotubes have been favored over metallic nanotubes, Lee et al. have demonstrated that metallic nanotubes can be the preferred pathway for charge transfer [21]. Qi et al. fabricated FETs with multiple tubes (20$\sim$30), which are still highly sensitive to chemical gating and generates lower electrical noise than individual tubes. Furthermore, they carried out polymer functionalization to increase the sensitivity for NO_2 detection.

In this thesis, an array of CNT FETs are fabricated and their conductances are monitored when exposed to NO_2. The sensor array acts as a CMOS interface for a chemical gas sensing system. A number of research groups have studied and modeled the molecular sensing mechanism for as-grown CNTs [22, 27, 30, 48], but the chemical and physical interactions between the gas molecules and the CNT sensor devices are not yet completely understood. The main objectives of this thesis are to characterize the resistive response of a whole sensor array, link the physics of gas adsorption to the electrical properties of CNT FETs, and understand the implications for system design.

Chapter 2

Characterizing Sensor Array

Gas adsorption on CNT sensors is studied through a large sensor array. This chapter describes the fabrication of CNT sensor devices and measurement setup for gas sensing experiments. Device variations and preliminary sensing response is discussed. Further details of the physics of gas adsorption and conductance change is modeled in the subsequent chapter.

2.1 Device Fabrication

Unlike CNT FETs designed for high-performance logic applications [15], the devices used here are rather simple FET geometries where the entire surface is exposed to the ambient. The nanotube, placed between two metal electrodes, is the channel of the FET and the devices are globally gated via the silicon substrate underneath the oxide layer.

Figure 2-1 shows a simplified diagram of the fabrication steps. Exact details of the fabrication procedures are omitted in this report since all lithography/metal-deposition steps are commonly used microfabrication processes. The final CNT FET structure is similar to those commonly reported in literature [7, 32]. The starting material is a p-type silicon wafer with a thin layer of thermal oxide on top. The first metal layer (Ti/Pt) is deposited to provide large metal pads for probing and to align CNT growth in subsequent steps. After depositing and patterning catalyst

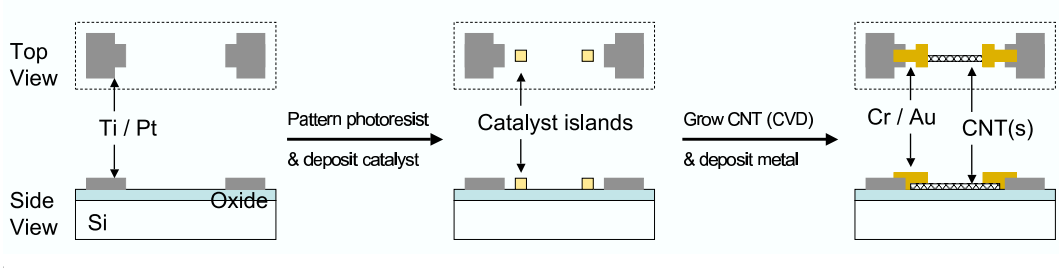

Figure 2-1: Schematic diagram of fabrication steps for CNTFET devices.

islands, CNTs are grown in a high-temperature furnace. Finally, a second metal layer (Cr/Au) is deposited to achieve good electrical contact to the nanotubes. The final device structure is shown in Figure 2-1 with a channel length of 4μm.

CNTs are grown via chemical vapor deposition (CVD), using an Fe/Mo-based catalyst and a CH_4 gas source at 900^oC [20]. The catalyst is deposited at pre-patterned sites within the array. After depositing the catalyst, the chip is placed in a CVD furnace, where CH_4 and Ar/H_2 are introduced. The critical growth conditions are consistent throughout this work.

Two chip designs were used in this report: a 14×7 and a 8×4 array. The former is used for device characterization and gas sensing responses, which are explained in Chapters 2 and 3. The latter is used for the CMOS-CNT system demonstration described in Chapter 4. Identical fabrication steps were used for both types of chips except that the 14×7 array was fabricated on a 500nm oxide wafer and the 8×4 array on a 100nm oxide wafer.

2.2 Device Variations

While the fabrication procedures presented in the previous section provide a systematic approach to building nanoscale materials for large-scale applications, current CNT growth is not completely controlled in terms of the diameter, type (metallic or semiconducting), and growth direction. Such inherent randomness to the growth procedures has important implications for device properties. In particular, the variations of the CNT diameter have been shown to play an important role on the metal-

nanotube interface resistance [7, 17]

2.2.1 Metal-Nanotube Contact

CNT FETs are known to operate as Schottky barrier (SB) transistors [12], and thus the metal-nanotube interface plays an important role in determining the electrical transport properties of a CNT FET. Thermionic emission and tunneling are involved in transport across the SB, which is sensitive to the contact metal work function. Very often the contact resistance dominates over channel conductance, this limits the potential of near-ballistic transport in CNT FETs. This has been a highly pursued area of research since it has significant implications for high-performance CNT device applications.

Javey et al. have suggested the importance of achieving both a high work-function metal and high quality metal-CNT interfaces to form low-barrier contacts [16]. Experimental work [7, 17] also indicates that the diameter of the nanotube is one of the most critical parameters in determining the CNT FET ON current for a given metal contact. Fundamentally, this diameter-dependence rises from the fact that the band gap of semiconducting CNTs varies inversely with diameter [29]. Smaller diameter CNTs have a higher band gap and thus a higher SB height. For large diameter CNTs ($\geq$ 2nm), Pd and Rh form negligible SBs to the p-channel [17].

In addition to the diameter dependence, the concept of Fermi-level pinning needs to be understood when considering SB heights for CNT FETs. Surface states exist at the interface of every material. These lead to surface dipoles for metallic surfaces, which contribute to the metal work function. For semiconductors, such surface states within the band gap lead to 'pinning' the Fermi level position of the semiconductor. For bulk metal-semiconductor interfaces, charge transfer between the two materials lead to band realignment, where a depletion width perpendicular to the interface is created. Thus, the SB height is generally fixed by Fermi-level pinning in bulk systems.

However, quasi one dimensional structures such as CNTs are much less sensitive to Fermi-level pinning. For example, Javey et al. have shown that the SB height shows a strong dependence on the metal work function of Pd, indicating the absence of

appreciable interface states between CNTs and Pd, and nearly no Fermi-level pinning [16]. For side-contacted CNTs, the CNT is covered axially by a metal layer and the whole semiconductor (i.e., CNT) is only a few nanometers thick in the direction perpendicular to the interface. For quasi-1D systems, the depletion width depends exponentially on doping [24]. At the nanoscale, band realignment is weak due to the limited available depletion width. In CNTs, this leads to relatively small and slowly varying SB with CNT diameters, which has important consequences when modeling the SB height. Both theoretical and experimental work is in agreement showing that a CNT contact to a high work function metal is unaffected by Fermi-level pinning, but controlled by the metal work function just as if there were no pinning and no interface dipole [25, 23].

2.2.2 Measurement Results

Characterizing the resistive properties of the devices within an array is important since the conductance change is monitored for gas sensing in this work. As discussed previously, the contact resistance and diameter distribution are likely a major source of variation. The CNT growth process is somewhat random and a number parameters can vary from device to device. The number of CNTs between the electrodes of each device can vary and each CNT can be either metallic or semiconducting, where semiconducting CNT FETs have a diameter-dependent band gap. These factors result in a rather large dynamic range of resistance values. After fabricating several chips, each device was probed using a semiconductor parameter analyzer (HP 4156A) under zero gating ($V_G = 0V$) and low-bias ($V_{DS} \simeq 50\sim100mV$). The measured resistance distribution for the as-grown CNT FETs is shown below.

Several steps can be made to reduce such variations. High quality electrical contacts can be made to reduce the SB height, and the kinetics of the CNT growth process can be controlled to yield a vary narrow diameter distribution of CNTs. While chirality of the CNT, and hence the type of the CNT cannot be effectively controlled to date, post-processing steps such as chemical treatments or electrical burn-out methods can be used to eliminate metallic CNTs. Such approaches have been readily

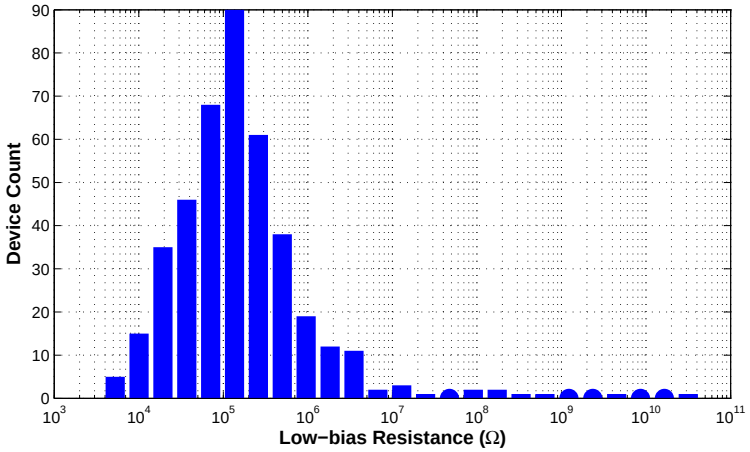

Figure 2-2: Histogram of low-bias resistance values. Part of the data was provided by Daniel Nezich. All devices were grown from a Fe/Mo-based catalyst with the same geometry (500nm oxide, 4μm channel, Cr/Au contacts).

demonstrated in research settings, but can become impractical for large-scale manufacturing. Furthermore, the extent to which device variations can be reduced is not yet fully known.

In this work, all sensor chips are used as-grown to achieve three main purposes: (1) study CNT sensors over a wide resistance range, (2) gain an understanding of the resistance change due to adsorption of gas molecules, and (3) demonstrate the need for variation-tolerant circuit schemes.

2.3 Sensor Array

The large variability among devices presents challenges when designing fully custom sensing applications. Many metal-oxide based sensors use reference electrodes to calibrate small device variations. In general, using an array of devices rather than a single source will increase reliability due to redundancy. In this chapter, the sensor response of the whole CNT array is characterized.

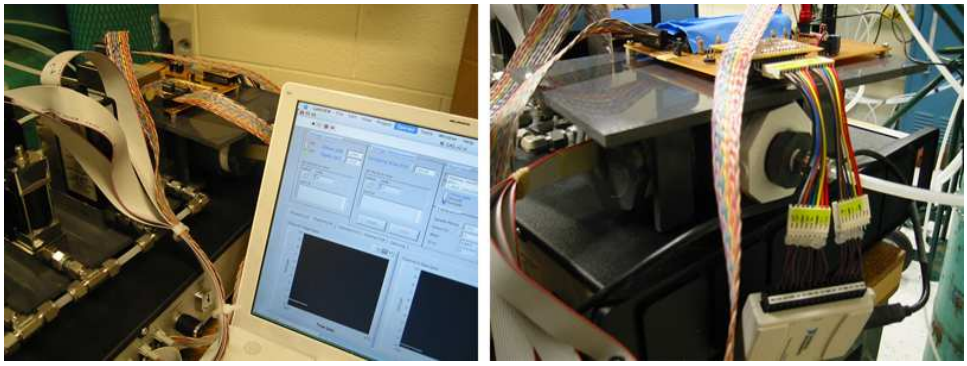

Figure 2-3: Setup used for gas sensing experiments. Mass flow controllers, gas chamber, and measurement circuitry are shown

2.3.1 Gas Experiment Setup

The gas sensing experiment setup is shown in Figure 2-3. All sensing experiments were conducted at room temperature and under atmospheric pressure. A simple T-shaped gas chamber was constructed out of poly-vinyl chloride (PVC). One end is connected as an inlet for the gas mixture to enter and another end as an outlet going into a fume hood. An electrical feedthrough was created to connect a sample holder residing within the chamber to an outside circuitry for sampling data.

The concentration of NO_2 was determined by modulating the flow rates of NO_2 and Ar. A pre-diluted mixture (1000ppm in Ar) was used for NO_2. Except for very low and high NO_2 concentrations, typical flow rates for Ar are 536 sccm. Given the available equipment, the flow rate of NO_2 was modulated from 10.61 to 216.57 sccm. The NO_2 concentration for sensing experiments presented in this work ranged from $\sim$10ppm to $\sim$1000ppm. The current-sensing circuitry was placed outside of the chamber and connected to a PC via a data-acquisition unit (DAQ) from National Instruments. A constant bias voltage was placed on the CNT FETs while the current signal was converted into a voltage signal and then sampled by the DAQ. Figure 2-4 shows the circuitry of the electrical measurement setup. This setup allows up to eight devices to be measured simultaneously. Sensing experiments were repeated for different devices on the same chip. Ample time (at least two days) was allowed for recovery for any given chip.

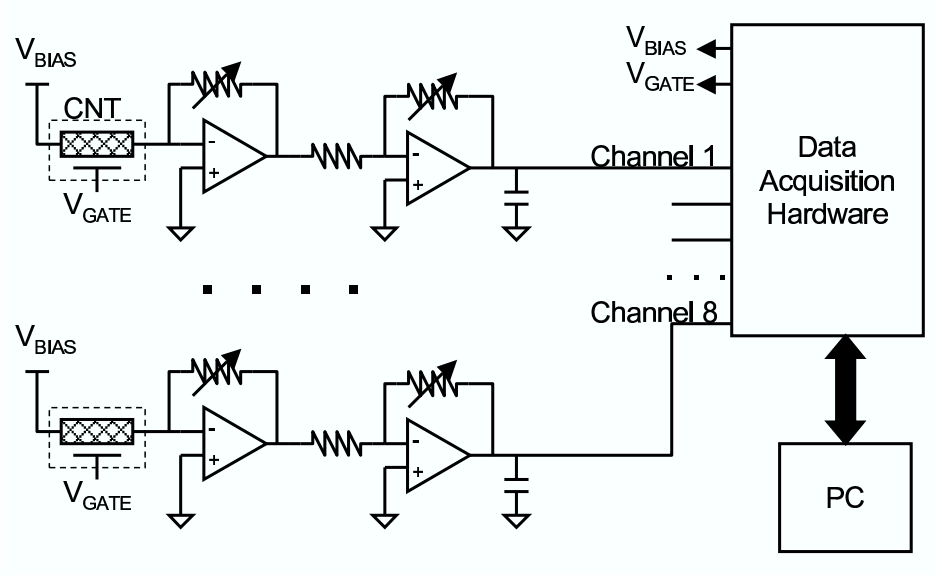

Figure 2-4: Schematic of the conductance measurement circuitry. A data-acquisition unit controls the bias and gate voltages of the CNT FETs, while a current-voltage converter relays the measured signal back to the PC.

2.3.2 Linear Sensing Response

The CNT array is used as-grown without any additional treatment. While the large dynamic range poses circuit challenges, characterizing the whole array as opposed to single devices can effectively increase the reliability of gas detection and identification. The following figure shows the resistance change (ΔR) as a function of initial resistance (R_0). Data points are collected all from the same chip. Although the $\Delta R - R_0$ response is linear on a large scale, large deviations exist when R_0 is small ($<400k\Omega$). Such effects can be understood by attributing the resistance change to two different sources, namely the metal contact and CNT surface, and further exploration of the limits of this linearity is discussed in Chapter 3.

While the initial resistance has been shown to vary over several orders of magnitude (Figure 2-2), Figure 2-5 shows that the amount of resistance change is roughly linear to the initial resistance and dependent on the gas concentration. This linearity is consistent to first order with other CNT sensor studies [21]. Although the large variation of initial resistance R_0 is generally undesirable, Figure 2-5 implies the lin-

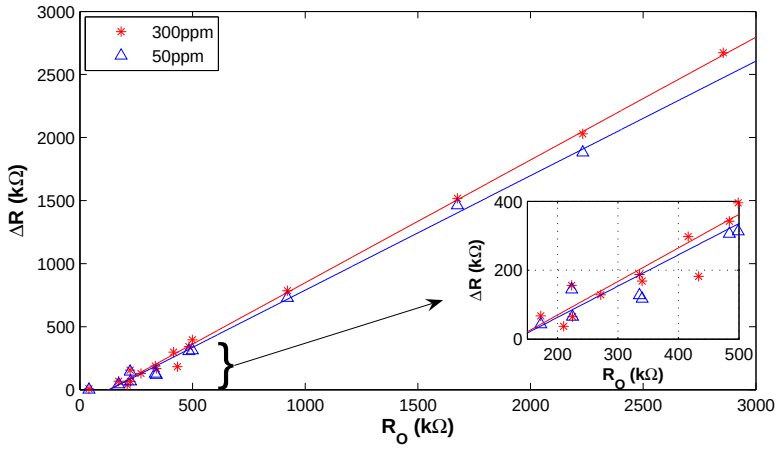

Figure 2-5: Resistance change upon NO_2 exposure. The response is largely linear, while large deviations exist for small R_0 values.

earity of $\Delta R - R_0$ rather than R_0 can be used as the mode for gas identification and characterization. FET-based sensors typically have a reference electrode for calibration, and are sensitive to ambient conditions and are known to change as time passes. Based on this linear response, array characterization of CNT sensors can be used as a reliable source for sensing application and potentially eliminate the need for device calibration since all devices are equally affected by external conditions.

2.3.3 Gating Effects

Kong et al. have demonstrated that the threshold voltage for CNT FETs are shifted upon adsorption of gas molecules, and higher sensitivity is achieved when FETs are gated [19]. CNT FETs are intrinsically p-type, and a positive gate voltage will deplete the device. Upon exposure to NO_2, the threshold voltage increases. The effects of gating are not extensively studied in this work, and most sensing experiments presented here are conducted under zero gate voltage. However, one would expect similar responses since gating simply modulates the Fermi level relative to the energy bands. Figure 2-6 shows the response of an identical device when back-gated.

In Figure 2-6-(a), the resistance change for back-gated devices is included along with the data presented in Figure 2-5. When a positive gate voltage is applied, the

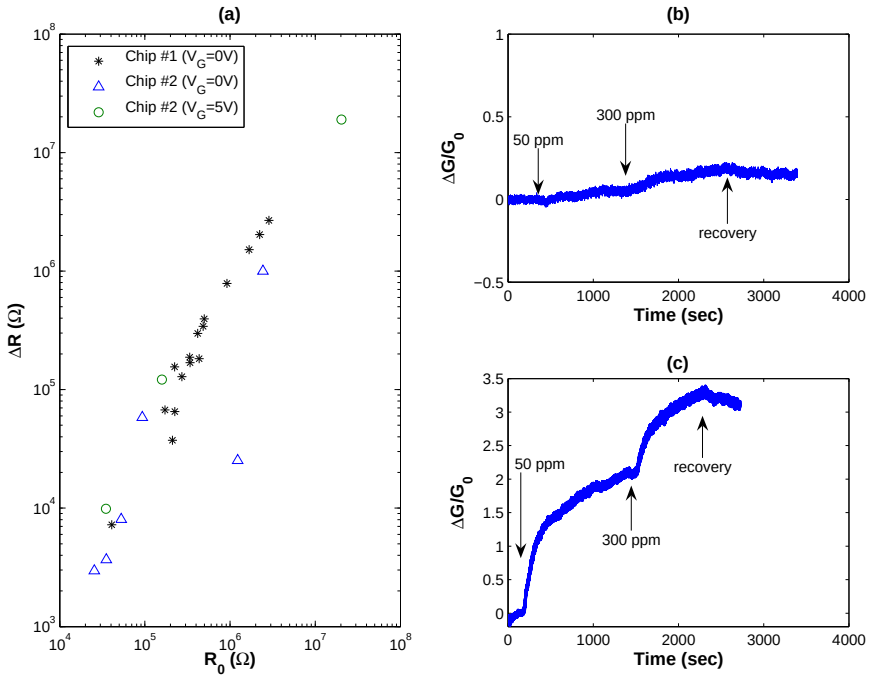

Figure 2-6: Effects of gating for exposure to NO_2 (300ppm) (a) Resistance change for various devices (b) Transient response with no gating (c) Transient response with gate voltage (5V) applied.

sensor devices are depleted, resulting in a much larger initial resistance. The $\Delta R - R_0$ data is still consistent with the original trend and falls along the linearly increasing curve. Figure 2-6-(c) shows that the amount of conductance change is much higher than that when no gating is applied (Figure 2-6-(b)). In addition, the sensor responds much faster when positive gating is applied. Thus, gating can be applied to effectively increase the sensitivity and decrease the response time, but give the same $\Delta R - R_0$ response.

Chapter 3

Understanding Gas Adsorption

This chapter includes detailed modeling of the response of the sensor array in connection to the underlying physics. The source of conductance change is examined, and an analytical model is derived to explain the sensor response. Finally, a set of new devices is presented to separate the effects of the metal contact and the nanotube upon gas adsorption.

3.1 Source of Conductance Change

The sensing response of CNTs is believed to come from a combination of nanotube channel doping and metal work function change. Depending on the gas of interest, reports vary on which effect dominates the sensing response. Bradley et al. suggests that NH_3 has a larger impact on the nanotube channel than the metal contacts [4], while H_2 and O_2 seem to change the metal work function [12, 16]. The effects of NO_2 have been widely studied but experimental results still suggest conflicting conclusions [19, 32, 35, 47, 42].

The key parameter connecting the electrical response to the physics of gas adsorption is the surface coverage (θ). Surface coverage is defined as the occupation probability of a particular gas molecule on a surface [46, 41]. The majority of the CNT sensor papers associate the conductance change (ΔG) directly to the surface coverage (i.e., $\Delta G \propto \theta$). This assumption fits certain sensing profiles fairly well but

fails to account for all effects. In this chapter, the surface coverage on the metal contact and the nanotube are treated separately.

3.1.1 Schottky Barrier Modulation Due to Gas Adsorption

Experimental work shows that gas adsorption on the metal contacts can alter the work function of the metal, thus affecting the energy alignments at the junction leading to the change in SB height [10, 16]. For example, when Pd-contacted CNT FETs are exposed to H_2, the Pd work function decreases and SB height increases for hole transport [16]. Doping can also be used to modify the SB height. Javey et al. have demonstrated CNT FETs with potassium (K) doped source and drain regions. Since Fermi level pinning is small or nearly absent in CNTs, they conclude that n-type contacts are formed as a result of SB height reduction and possibly SB width thinning [15]. In addition to local work function changes, more complex short-range interactions between CNT and gas molecules can also influence transport properties. A general approach of relating the SB height to the conductance is taken in this work.

Since CNT FETs are intrinsically p-channel FETs, the difference between the metal work function and CNT valence band in reference to vacuum level determines the SB height. The p-channel SB height is [7, 17]:

$$\Phi_0 = \left(\phi_{CNT} + \frac{E_g}{2}\right) - \phi_M \tag{3.1}$$

where ϕ_{CNT}= 4.7 eV [10], and E_g and ϕ_M are the band gap and metal work function respectively. Since little Fermi level pinning exists at the metal-nanotube interface [16, 25], this classical formalism is able to describe the qualitative trends. As discussed in Chapter 2.2.1, quasi-1D electrostatics dictates a much more slowly varying SB height dependence on CNT diameter than expected from equation 3.1. Thus, a more accurate approximation presented by Lèonard and Talin is used here [23]. The SB height is given as:

$$\Phi_{SB} \approx \frac{kT}{\beta} \ln\left(\frac{\alpha\sqrt{\frac{E_g}{2kT}}}{\ln\alpha\sqrt{\frac{E_g}{2kT}} - \frac{\Phi_0}{kT}}\right) \tag{3.2}$$

where Φ_0 is given in equation 3.1, and after simplifying the expressions in [23], $\alpha = \frac{e^2\left(\frac{2}{\pi}\right)^{\frac{3}{2}}}{3\sqrt{\beta a\gamma dC}}$ ($\beta = 0.7$, $a = 0.142$ nm C-C bond length, d = CNT diameter, $\gamma = 2.5$eV is tight-binding overlap integral, e = the electron charge, k = Boltzmann factor, $T = 300$K, and C = capacitance per unit area between metal-CNT). Assume an initial ($\Phi_{SB.i}$) and final SB ($\Phi_{SB.f}$) before and after gas adsorption. Also assume that the band gap of the CNT does not change after gas adsorption, then the following expression becomes:

$$\begin{aligned}
exp\left[\frac{\Delta\Phi_{SB}}{kT}\right] &= exp\left[\frac{\Phi_{SB.f} - \Phi_{SB.i}}{kT}\right] \\
&= exp\left[\frac{1}{\beta}\ln\left(\frac{\alpha\sqrt{\frac{E_g}{2kT}}}{\ln\alpha\sqrt{\frac{E_g}{2kT}} - \frac{\Phi_{0.f}}{kT}}\right) - \frac{1}{\beta}\ln\left(\frac{\alpha\sqrt{\frac{E_g}{2kT}}}{\ln\alpha\sqrt{\frac{E_g}{2kT}} - \frac{\Phi_{0.i}}{kT}}\right)\right] \\
&= exp\left[\frac{1}{\beta}\ln\left(\frac{\ln\alpha\sqrt{\frac{E_g}{2kT}} - \frac{\Phi_{0.i}}{kT}}{\ln\alpha\sqrt{\frac{E_g}{2kT}} - \frac{\Phi_{0.f}}{kT}}\right)\right] \\
&= \left[\frac{\ln\alpha\sqrt{\frac{E_g}{2kT}} - \frac{\Phi_{0.i}}{kT}}{\left(\ln\alpha\sqrt{\frac{E_g}{2kT}} - \frac{\Phi_{0.i}}{kT}\right) - \frac{\Phi_{0.f} - \Phi_{0.i}}{kT}}\right]^{\frac{1}{\beta}} \\
&= \left[\frac{1}{1 - \frac{\Delta\Phi_0}{kT\cdot\left(\ln\alpha\sqrt{\frac{E_g}{2kT}} - \frac{\Phi_{0.i}}{kT}\right)}}\right]^{\frac{1}{\beta}}
\end{aligned} \tag{3.3}$$

Furthermore, the SB height change can be attributed to the change in Φ_0. In particular, the work function of metals is known to change when gas molecules are adsorbed on the surface. A surface dipole layer forms on the metal surface causing polarization of the molecule. Evidence suggests that there is a linear relation between $\Delta\phi_M$ and surface coverage for certain molecules, while extreme non-linearities exist for others [13, 33, 46, 41]. Furthermore, if one assumes a Helmholtz layer type

approximation, then the amount of charge transfer is approximated as directly proportional to the polarizability, dipole moment, and surface coverage. Understanding details of surface orientation, metal contact geometry, and gas adsorbate is crucial to modeling the gas-surface reaction. However, little data is found in literature on the nature of NO_2 adsorption and detailed studies of NO_2 adsorption on metal surfaces is beyond the scope of this work. To first order, a reasonable approximation is to assume a simple linear relation between Φ_0 and the surface coverage at the metal surface (θ_M). This approach is taken here, which then simplifies equation 3.3 to:

$$exp\left[\frac{\Delta\Phi_{SB}}{kT}\right] = (1 - b\theta_M)^{-\frac{1}{\beta}} \tag{3.4}$$

where b is a constant dependent on: $b \propto \frac{1}{kT\cdot\left(\ln\alpha\sqrt{\frac{E_g}{2kT}} - \frac{\Phi_{0,i}}{kT}\right)}$. The polarizability and dipole moment of the gas molecule will determine whether b is positive or negative, which corresponds to either an decrease or increase in conductance.

3.1.2 Charge Transfer to Nanotube

Charge transfer doping is much stronger for CNTs than planar devices due to quasi-1D electrostatics [24]. Several reports [3, 18] show that ΔG is caused by charge transfer from analyte molecules adsorbed on the CNT surface, and such layers also form a polarizable layer that increases the CNT FET capacitance. Certain gas molecules - acetone, NH_3, and CH_4- have been calculated to interact weakly with minimal charge transfer with CNTs [5, 49].

The CNT sensor response to NO_2 has also been heavily researched. While the acceptor nature of NO_2 is widely accepted, Santucci et al. suggest that the NO_2-CNT bonding is rather weak [35], implying that the charge transfer is not the leading sensor mechanism of CNTs as suggested in [6, 19]. Rather, the experimental trends - increasing conductance upon NO_2 exposure- are attributed to density of states (DOS) modifications. The hole conductivity is suggested to increase as a result of increased population of NO_2 adsorbates acting as charge acceptors, albeit a small binding energy. Zhang et al. has conducted NO_2 sensing experiments with passivated layers to

isolate effects on the metal/nanotube. They conclude that the charge transfer between NO_2-CNT is immeasurable and that the interface properties (i.e., SB) dominates the sensor response. Similar experiments presented here (Section 3.3) and in [26] are in agreement with this SB-dominated sensing mechanism for NO_2, but also offer evidence that charge transfer between NO_2-CNT is measurable and can still be quite dominant.

The nature of such diverse conclusions seem to suggest that there are several factors that are normally overlooked or where the combined effect is difficult to quantify: geometry of metal pads, length of CNT channels, inter-tube interaction in CNT bundles, defects sites, surface dipole interactions at the metal, non-uniform charge distribution inside the nanotube, the quality of CNTs, etc. The effects of defects have been widely studied and are known to affect charge transfer and adsorption properties [1, 11, 44]. Modeling all the above effects is daunting. However, a simple phenomenological model can be applied which is commonly used in literature but still capturing the most important dependence: relating the conductance to the adsorption of gas molecules to the CNT. The same site-binding description is used here as in [22], where each atom along the nanotube surface is modeled as a binding site for molecular adsorption. Assuming that the charge carrier density (n) is proportional to the available binding sites, the surface coverage on the CNT (θ_{NT}) dictates how much of those binding sites are occupied and results in the conductance change. Thus, for a final and initial carrier density of n_f and n_0 respectively (δ is a proportionality constant):

$$Occupied\ Binding\ Sites \propto n_f - n_0$$

$$Total\ Binding\ Sites \propto n_0$$

$$\theta_{NT} = \frac{Occupied\ Binding\ Sites}{Total\ Binding\ Sites} \propto \frac{n_f - n_0}{n_0}$$

$$\delta\theta_{NT} = \frac{n_f - n_0}{n_0}$$

$$\frac{n_0}{n_f} = \frac{1}{\delta\theta_{NT}+1} \tag{3.5}$$

3.2 Modeling Gas Adsorption

Most papers found in literature attribute the change in conductance (ΔG) simply to the surface coverage [21, 22, 32]. While this approach may be viable in certain cases, the effect of the SB modulation is overlooked. Suehiro et al. used Al-contacted CNT FETs that form large barriers [42]. High contact-resistance devices elucidate the nature of SB modulation, which suggest that the total resistance needs to be modeled as the sum of the contact resistance (R_M) and the CNT channel resistance (R_{CNT}), instead of only considering the CNT channel conductance.

However, due to the stochastic nature of CNT growth, the exact composition and number of tubes for each sensor device cannot be easily quantified. In addition, CNT devices typically used in sensor studies are not perfectly aligned and in many cases a CNT-film is used. Defects along the CNT can also affect the energy gap at the Fermi level in semiconducting CNTs and the density of states at the Fermi level in metallic CNTs [11]. Fortunately, the ensemble of metallic and semiconducting CNTs in a device, whether in a FET structure or a thin film, appears to share similar features to that of semiconducting devices [32, 38].

Hence, the effects discussed in the previous section are directly used here. Assume an initial and final resistance as $R_0\,(= R_M + R_{CNT})$ and $R_f\,(= R_{M.f} + R_{CNT.f})$, respectively, then the CNT resistance will be inversely proportional to the carrier density ($R_{CNT} \propto \frac{1}{n_0}$). Under a fixed bias voltage, the current density through a SB is generally exponentially dependent on the SB height and is proportional to the carrier density. Thus, $R_M \propto \frac{1}{n_0} e^{\frac{\Phi_{SB.0}}{kT}}$. Then, using equation 3.4 and 3.5, the total resistance change becomes:

$$\begin{aligned}\Delta R &= R_f - R_0 \\ &= R_M \cdot \left(\frac{R_{M.f}}{R_M} - 1\right) + R_{CNT} \cdot \left(\frac{R_{CNT.f}}{R_{CNT}} - 1\right)\end{aligned}$$

$$
\begin{aligned}
&= R_M\left[\frac{n_0}{n_f}e^{\frac{\Delta\Phi_{SB}}{k_BT}}-1\right]+R_{CNT}\left[\frac{n_0}{n_f}-1\right] \\
&= R_M\left[\left(\delta\theta_{NT}+1\right)^{-1}\left(1-b\theta_M\right)^{-\frac{1}{\beta}}-1\right]+R_{CNT}\frac{-\delta\theta_{NT}}{\delta\theta_{NT}+1} \qquad (3.6)
\end{aligned}
$$

$$
\begin{aligned}
\frac{\Delta G}{G_0} &= \frac{G_f-G_0}{G_0} \\
&= \frac{G_f}{G_0}-1 \\
&= \frac{R_0}{R_f}-1 \\
&= \frac{R_0-R_f}{R_f} \\
&= \frac{-\Delta R}{R_0+\Delta R} \\
&= \frac{\left[1-\left(\delta\theta_{NT}+1\right)^{-1}\left(1-b\theta_M\right)^{-\frac{1}{\beta}}\right]R_M+\frac{\delta\theta_{NT}}{\delta\theta_{NT}+1}R_{CNT}}{\left(\delta\theta_{NT}+1\right)^{-1}\left(1-b\theta_M\right)^{-\frac{1}{\beta}}R_M+\frac{1}{\delta\theta_{NT}+1}R_{CNT}} \qquad (3.7)
\end{aligned}
$$

Now, the surface coverage, θ_M and θ_{NT} are obtained through the Langmuir model. A Langmuir isotherm assumes a monolayer coverage of gas molecules on the surface. The site-binding model presented in [22] exactly resembles a Langmuir isotherm and shares the same mathematical form. This interpretation is consistent with experimental data showing that conductance change eventually saturates with increasing concentration of the gas molecules [34]. The transient and steady-state response of the surface coverage in a Langmuir isotherm is readily given as [41, 46]:

$$\theta_M = \left(1-e^{-k_MPt}\right) \qquad (3.8)$$

$$\theta_{NT} = \left(1-e^{-k_MPt}\right) \qquad (3.9)$$

$$\theta_M = \frac{K_MP}{K_MP+1} \qquad (3.10)$$

$$\theta_{NT} = \frac{K_{NT}P}{K_{NT}P+1} \tag{3.11}$$

where t is time (sec), P is the partial pressure of NO_2 (Pascal), $k_{M,NT}$ is the adsorption rate constant ($Pascal^{-1}s^{-1}$), and $K_{M,NT}$ is the Langmuir constant ($Pascal^{-1}$). Using parameters found in [32], the adsorption and desorption equilibrium of NO_2 results in ($E_{b.M}$ and $E_{b.NT}$ are the NO_2 binding energies to the metal and CNT surface respectively):

$$K_M = \frac{S\sigma}{\sqrt{2\pi mkT}\nu} e^{\frac{E_{b.M}}{kT}} \tag{3.12}$$

$$K_{NT} = \frac{S\sigma}{\sqrt{2\pi mkT}\nu} e^{\frac{E_{b.NT}}{kT}} \tag{3.13}$$

3.3 Application to Data

3.3.1 Parameter Variation

The relative strengths of the surface interaction between the gas molecule and the metal/CNT will determine which effect dominates the sensor response. The binding energies in large determine the Langmuir constants (K_M and K_{NT}), which then determine how quickly the surface coverage converges to $\sim$1 as a function of partial pressure. The proportionality factors (b and δ) determine the strength of the surface interaction and ultimately the saturation point of $\Delta G/G_0$.

Figure 3-1 shows the dependence of $\Delta G/G_0$ as a function of binding energy, assuming values of b=-1, δ=1, and an initial resistance where R_M/R_{CNT}=1. At a given concentration, $\Delta G/G_0$ is roughly constant at low and high binding energies, and shows a sharp increase in between. This plateauing at large binding energies occurs since the surface coverage quickly converges to one for binding energies above a critical value. At small binding energies, the surface coverage is nearly zero and hence the effect of increasing the binding energy does not alter the conductance response by a large amount.

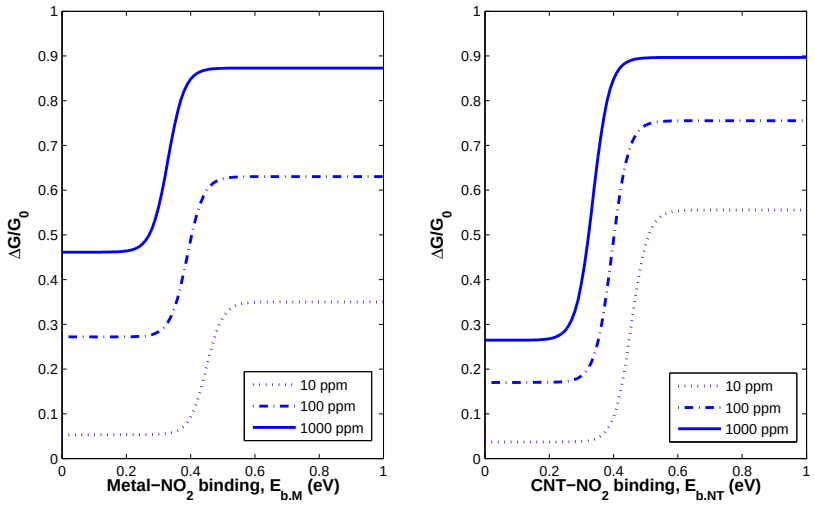

Figure 3-1: Dependence on surface binding energies. Assuming values of b=-1, δ=1, and $R_M/R_{CNT} = 1$

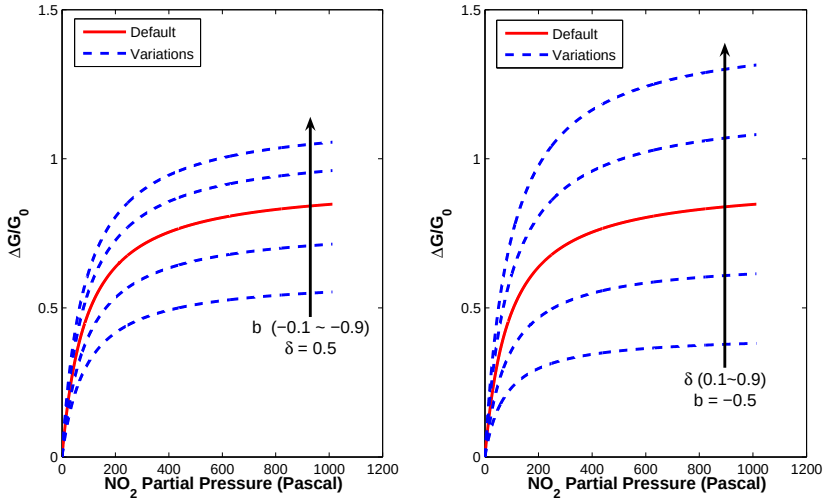

Figure 3-2: Dependence on b and δ. Assuming default values of $E_{b.M}$=0.4eV, $E_{b.NT}$=0.4eV, b=-1, δ=1, and R_M/R_{CNT}=1

Figure 3-2 shows the effects of b and δ on $\Delta G/G_0$. The constant factors, b and δ are related to the dipole polarizability and charge transfer respectively. Increasing the magnitude of these factors (b is negative) increases the maximum $\Delta G/G_0$ value. This saturation point of $\Delta G/G_0$ increases non-linearly as a function of b because of the non-unity β factor. If the sensing response is dominated by the metal contact, one can assume that charge transfer is negligible (i.e., $\delta \rightarrow 0$). Conversely, if the surface interactions at the CNT surface dominate the sensing response, the dipole moment or the polarizability at the metal contact can be ignored (i.e., $b \rightarrow 0$). From equation 3.7, the sensing response at either limit simplifies to:

$$Metal\ contact\ dominated: \quad \frac{\Delta G}{G_0} \simeq \frac{\left[1-(1-b\theta_M)^{-\frac{1}{\beta}}\right] R_M}{(1-b\theta_M)^{-\frac{1}{\beta}} R_M + R_{CNT}} \tag{3.14}$$

$$(R_M >> R_{CNT}) \quad \rightarrow \quad (1-b\theta_M)^{\frac{1}{\beta}} - 1 \tag{3.15}$$

$$CNT\ dominated: \quad \frac{\Delta G}{G_0} \simeq \delta\theta_{NT} \tag{3.16}$$

If charge transfer between the CNT and gas molecule is the leading sensing mechanism, the above relation shows that the normalized conductance change is roughly constant at a given concentration. In other words, the conductance change is directly proportional to the initial conductance, which is consistent with the site-binding model presented in [22, 21]. The initial conductance is assumed to be proportional to the number of nanotubes within each device. A larger number of nanotubes relates to a larger number of binding sites and hence a higher chance of surface binding and charge transfer to occur. If the transient form of θ is taken (equation 3.8 and 3.9), note that equation 3.16 exactly reduces to the form of the equation presented in [21], where $\delta = \left(\frac{\Delta G}{G_0}\right)_{max}$.

The exact composition of R_M and R_{CNT} is difficult to quantify and will vary severely from device to device. Nonetheless, as evident from Chapter 2, the metal contact resistance is known to vary over a much wider dynamic range than the channel resistance. The CNT channel resistance is expected to be fairly small, $\sim 50k\Omega$, and de-

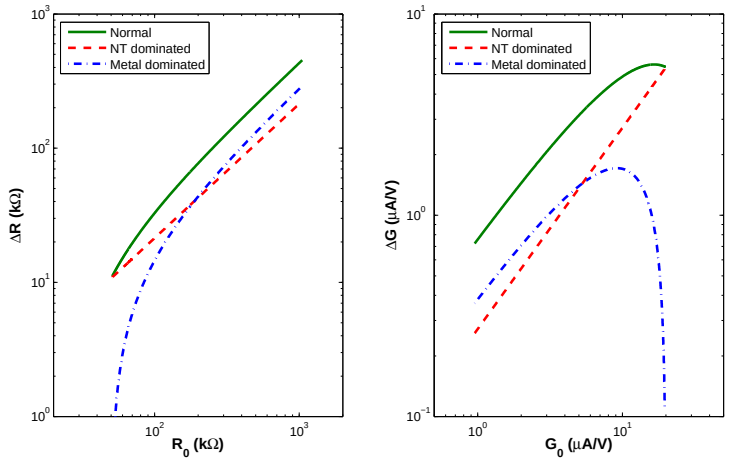

Figure 3-3: Resistance (Conductance) change as a function of initial resistance (conductance). Assumes a fixed R_{CNT}=50$k\Omega$ and exposure to 100 ppm NO_2. Normal conditions use values of $E_{b.M}$=0.4eV, $E_{b.NT}$=0.4eV, b=-0.5, and δ=0.5. Either b or δ is set to zero in the limiting case.

vices with multiple nanotubes will only decrease the effective CNT channel resistance. Figure 3-3 assumes a fixed value of R_{CNT}=50$k\Omega$ (i.e., $R_0 = R_M + 50k\Omega$) and plots the change in resistance/conductance as a function of the initial resistance/conductance. From equation 3.16, the CNT-dominated sensor response (for $\Delta G/G_0$) is strictly a linear curve and is confirmed in Figure 3-3. The metal-dominated sensor curve is also a linear function (for $\Delta R - R_0$), but with a non-zero intercept value. Hence, when plotted on a log-log scale, the response is mostly linear but curves down for small values of R_0. This apparent non-linearity is highlighted when plotting the conductance change ($\Delta G - G_0$) on a log-log scale.

Figure 3-4 shows the conductance response of a few sensor devices on a log-log scale. The NO_2 sensing response is from the same data presented in Figure 2-5. The two other devices are referenced in [21]. Lee et al. sense thionyl chloride ($SOCl_2$) and dimethyl methylphosphonate (DMMP). Two types of CNT samples are prepared in a suspension using sodium dodecyl sulfate (SDS) or DNA ($d(GT)_{15}$). These sensors fit an exact linear profile and are indicative of a CNT-dominated sensing mechanism, which is consistent with their report. The NO_2 sensing curve exhibits non-linearities reminiscent of a metal-dominated sensing mechanism. The data points were fit to

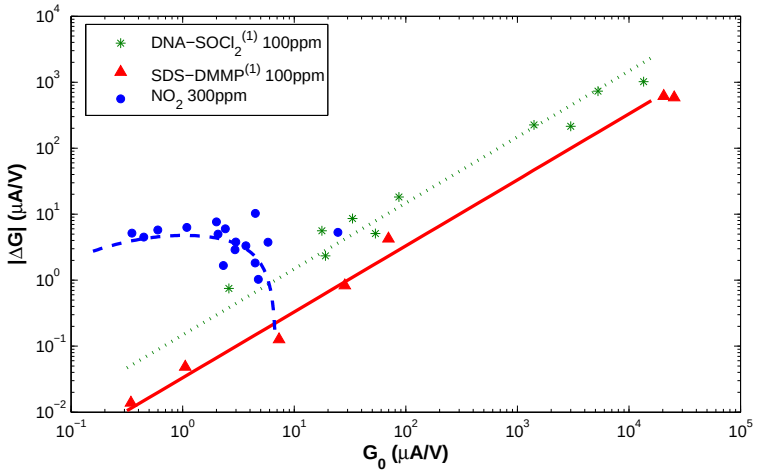

Figure 3-4: Experimental data on ΔG vs. G_0. Lines represent data fits. NO_2 fit assumes values of $E_{b.M}$=0.8eV, $E_{b.NT}$=0.43eV, b=-10, and δ=0.05. (1) Data from [21]

a curve with a higher metal-NO_2 interaction: b=-10 and δ=0.05. These results are consistent with recent findings, suggesting that NO_2 sensing is dominated by interface properties at the metal contact [47].

3.3.2 Al-contacted Devices

To understand the dependence on metal, new devices are fabricated using similar procedures outlined in Chapter 2 except that the final contact metal is Al instead of Cr/Au. Al-contacts are known to form high SB (and thus higher resistance) devices [7] due to the low work function of Al. Figure 3-5 shows the $\Delta R - R_0$ response for the standard Cr/Au and Al-contacted devices. The results for Al-contacted devices are from repeated measurements under both zero and positive gate voltages applied. The linearity of $\Delta R - R_0$ extends for very large resistance values.

Figure 3-6 shows the transient response of Al-contacted devices. Similar to [42], Al-contacted devices respond much faster to NO_2 than the Cr/Au devices. However, unlike [42], the conductance (resistance) of the Al-contacted device increases (decreases) monotonically instead of showing an initial burst of conductance decrease (resistance increase). This discrepancy can be attributed to several factors. The devices presented in [42] use Cr/Al metal contacts, and the sampling rate is much higher

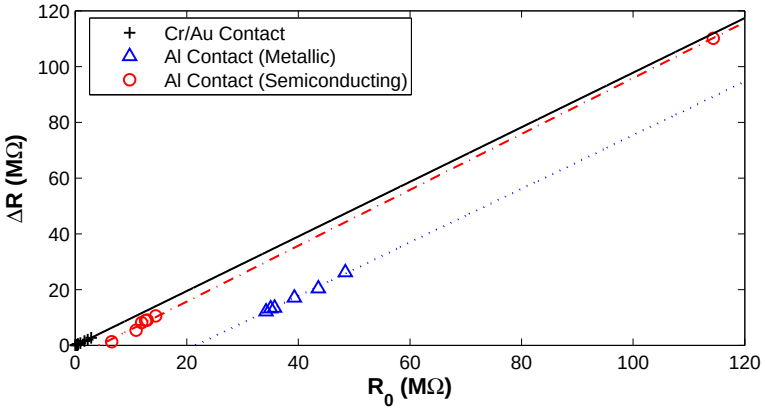

Figure 3-5: Resistance response for Al-contacted devices exposed to 300ppm NO_2.

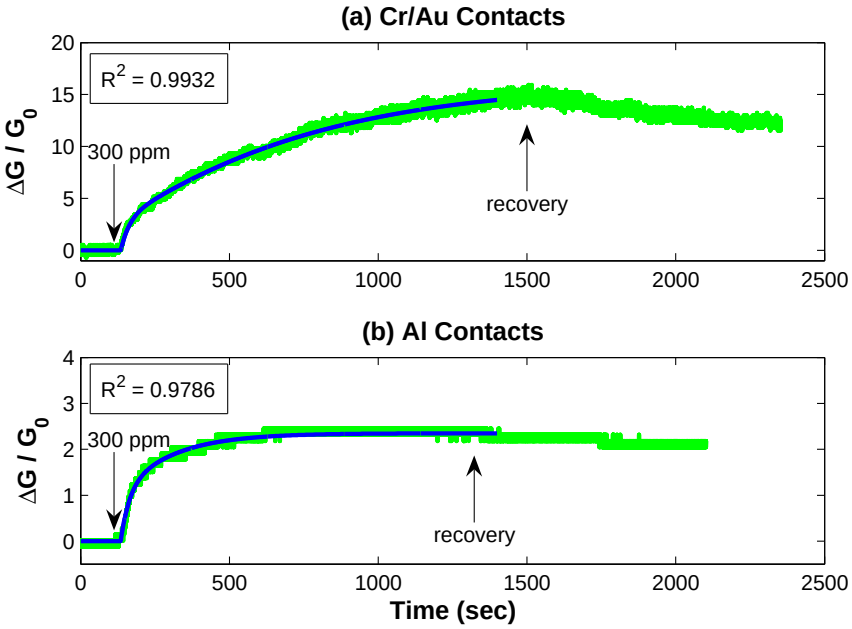

Figure 3-6: Transient response to 300ppm NO_2 for (a) Cr/Au and (b) Al-contacted device.

Table 3.1: Fitting parameters for Figure 3-6

	b	δ	k_M (Pascal^{-1}s^{-1})	k_{NT} (Pascal^{-1}s^{-1})	Goodness of fit
Cr/Au	-1.77	3.011	5.793×10^{-5}	1.293×10^{-3}	0.9932
Al	-0.3897	1.093	1.981×10^{-4}	1.271×10^{-3}	0.9786

(100 kHz). Figure 3-6 also shows fitted curves. Both devices presented in the figure are semiconducting CNTs and have a high initial resistance: 2.8MΩ for the Cr/Au device, and 12MΩ for the Al device. Thus, in the limit that the CNT resistance is negligible compared to the contact resistance ($R_M >> R_{CNT}$), equation 3.7 becomes:

$$\frac{\Delta G}{G_0} \simeq (\delta\theta_{NT} + 1)\,(1 - b\theta_M)^{\frac{1}{\beta}} - 1 \tag{3.17}$$

where the transient form of θ is used (equation 3.9 and 3.8). The curves fit very well to the data, better than the standard form of $\Delta G/G_0 \simeq \theta$. Recall that b and δ can vary from device to device since the effective band gap, number of nanotubes, and mixture of metallic and semiconducting nanotubes is different. However, one can expect that the CNT adsorption rate constants (k_{NT}) will be more or less similar for both devices. Table 3.1 shows the curve fitting parameters, and indeed the CNT adsorption rate is roughly 1.3×10^{-3} Pascal^{-1}s^{-1} for both devices. Also, the metal adsorption rate is roughly an order magnitude higher for Al than Cr/Au, which is also consistent with [42].

3.3.3 Partially Exposed Devices

To further understand the impacts of the metal contact and nanotube, two types of new devices are fabricated: CNT-exposed and contact-exposed devices. Similar to previous experiments [26, 47], the CNT/contact-exposed devices are fabricated by taking the standard (fully-exposed) devices fabricated previously and coating a layer of poly methyl methacrylate (PMMA), and then exposing certain regions by e-beam lithography. However, unlike [26], the contact-exposed devices presented here only

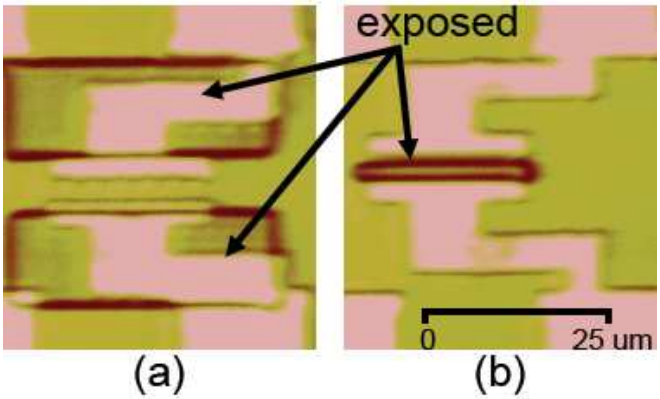

Figure 3-7: Optical image of (a) contact-exposed and (b) CNT-exposed devices.

expose the metal contacts and not the metal-nanotube interface regions. Figure 3-7 shows optical images of the PMMA-exposed devices, and Figure 3-8 shows the transient response of these devices when exposed to NO_2. Several other devices have been tested and showed similar responses.

The CNT-exposed device shows a similar response to the fully-exposed device, but the contact-exposed device appears to take a longer time to respond to NO_2. This indicates that surface binding upon the metal is rather weak, and that the long saturation time is due to NO_2 diffusion through the PMMA layer. This result does negate the previous conclusion that the metal-NO_2 interaction might be the dominant sensing mechanism, but implies that the SB height modulation is dominated by the CNT valence band lineup rather than the metal work function change, and that charge transfer or other surface interactions right at the vicinity of the metal-CNT interface might play an important role.

Liu et al. present similar devices but report that diffusion of NO_2 or NH_3 through the PMMA layer was negligible [26]. However, Zhang et al. also conducted similar experiments but concluded that the conductance change in CNT-exposed devices is due to NO_2 diffusing through PMMA and interacting with the metal [47]. The initial resistance of their device at zero gate voltage is extracted from the gate sweep, which is roughly 700$\sim$800kΩ. Furthermore, Zhang et al. only exposed one-third of the CNT channel. The CNT-exposed device presented here is also a semiconducting nanotube

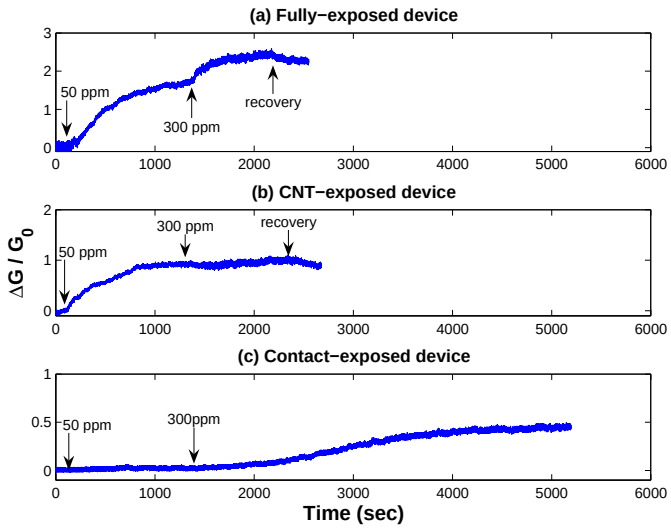

Figure 3-8: Transient response of a (a) fully-exposed (b) CNT-exposed and (c) contact-exposed device upon exposure to 50ppm and 300ppm NO_2. Light-colored lines represent the experimental data and dark-colored lines represent fitted curves.

but has a small initial resistance ($\sim$150kΩ) and most of the CNT channel ($\sim$90%) is exposed. While Zhang et al. conclude that charge transfer at the CNT surface has little effect, the CNT-exposed device presented here (Figure 3-8) clearly indicates that conductance modulation through CNT-NO_2 binding is still quite significant. This discrepancy might be attributed to the difference in the (metal contact) resistance values and the amount of CNT channel exposure. Devices fully covered with PMMA are needed to further investigate the effect of PMMA diffusion, and such experiments remain as future work.

Figure 3-9 shows two contact-exposed devices exposed to 300ppm NO_2. The time to fill up the gas chamber is on the order of 80$\sim$100 seconds, which is significantly less than the typical response time of the sensor devices presented in this thesis. Thus, one can approximate a constant concentration of NO_2 right on the outer surface of PMMA. Assuming a constant surface concentration, diffusion through a layer is given as [31]:

$$C(t) = C_0 \times erfc\left(\frac{d_{pmma}}{2\sqrt{Dt}}\right) \tag{3.18}$$

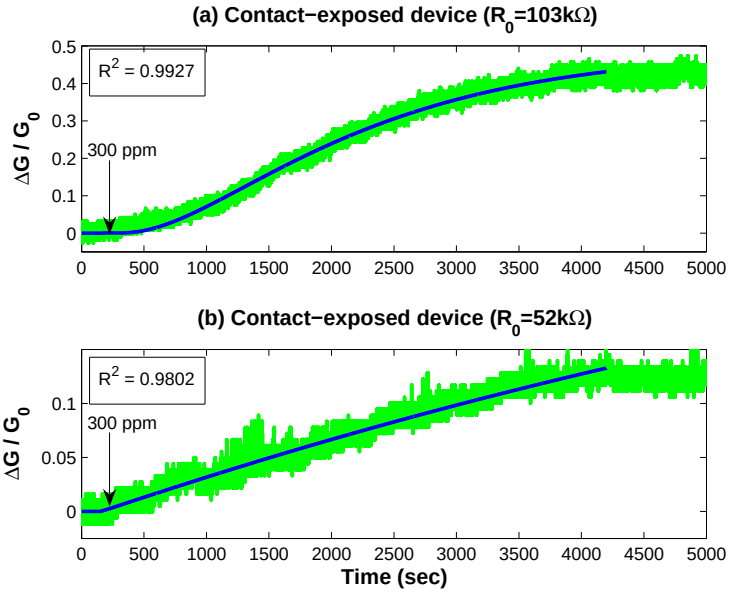

Figure 3-9: Transient response of contact-exposed devices, where (a) R_0=103kΩ and (b) R_0=52kΩ, exposed to 300ppm NO_2. Light-colored lines represent experimental data, and dark-colored lines are fitted curves.

where C_0 is the concentration at the surface, t is time, d_{pmma} is the thickness of the PMMA layer, D is diffusivity of NO_2 through PMMA, and $erfc$ is the complementary error function given as: $erfc(x) = 1 - \frac{2}{\pi}\int_0^x e^{-\eta^2} d\eta$. Given this approximation, equations 3.7 and 3.8 can be used to fit the experimental data. In particular, instead of a static concentration value, a time varying form described in 3.18 is used for CNT-NO_2 binding.

3.3.4 Surface Binding

The surface binding energies of NO_2 to the metal and CNT can be found by fitting curves to $\Delta G/G_0$ as a function of partial pressure of NO_2. The steady-state form of the surface coverage (equations 3.11 and 3.10) is used. Dev #1/2/3 presented in this section refer to the standard Cr/Au-contacted, fully-exposed devices. Al-Dev #1,2 refer to the Al-contacted devices. Figure 3-10 shows the curve for the CNT-exposed (Cr/Au-contacted) device. This assumes the functional form of equation 3.16 where only the interaction with the nanotube plays a role (i.e., b $\rightarrow$ 0). The fitting

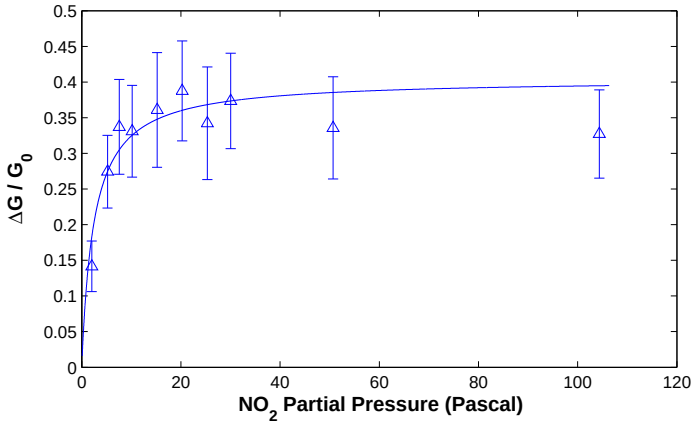

Figure 3-10: Pressure dependence of a CNT-exposed device. Lines represent fitted curves.

Table 3.2: Fitting parameters for $\Delta G/G_0$ as a function of pressure. Curves shown in Figures 3-10, 3-11, and 3-12

	b	δ	K_M (Pascal^{-1})	K_{NT} (Pascal^{-1})	R_M/R_{CNT}	Goodness of fit
Dev #1	-0.2565	0.2436	1.572	1.579	-	0.6239
Dev #2	-0.0020	2.0669	7999	0.1301	0.1986	0.9802
Dev #3	-0.0030	0.3103	651.5	0.0208	0.0007	0.9582
Al-Dev #1	-0.7886	0.4605	0.0040	0.6928	-	0.9507
Al-Dev #2	-0.762	0.7006	1.546	1.56	-	0.8777
CNT-exposed	-	0.4041	-	0.4061	-	0.8995
PEI-coated	-229.1	0.0011	30.75	5247	0.5868	0.9795

parameters for all figures in this section are listed in Table 3.2.

For Al-contacted devices, the same approximation in equation 3.17 is used ($R_M >> R_{CNT}$). Figure 3-11 shows the data points. A similar approach was taken for Dev #1 in Figure 3-12-(a). The most general equation (3.7) was used for Dev #2 and #3. Qi et al. present similar CNT devices with Mo metal contacts [32]. Coating the devices with polyethyleneimine (PEI) turns them into n-type FETs and effectively increases the sticking probability by 2 orders of magnitude. The conductance response is shown in Figure 3-12-(b). Note that the range of partial pressure is 3∼4 orders of magnitude less then the standard devices, indicating higher sensitivity.

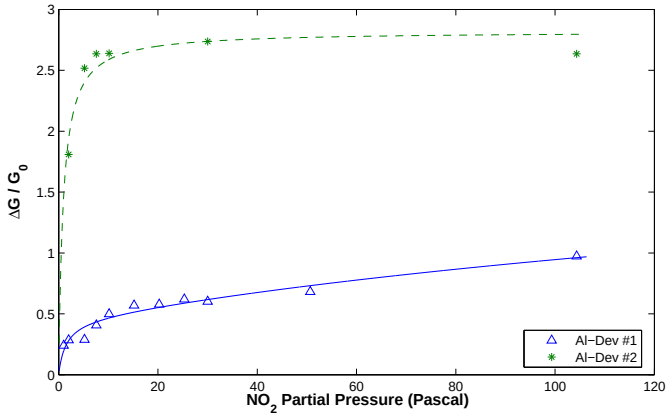

Figure 3-11: Pressure dependence of Al-contacted devices. Lines represent fitted curves.

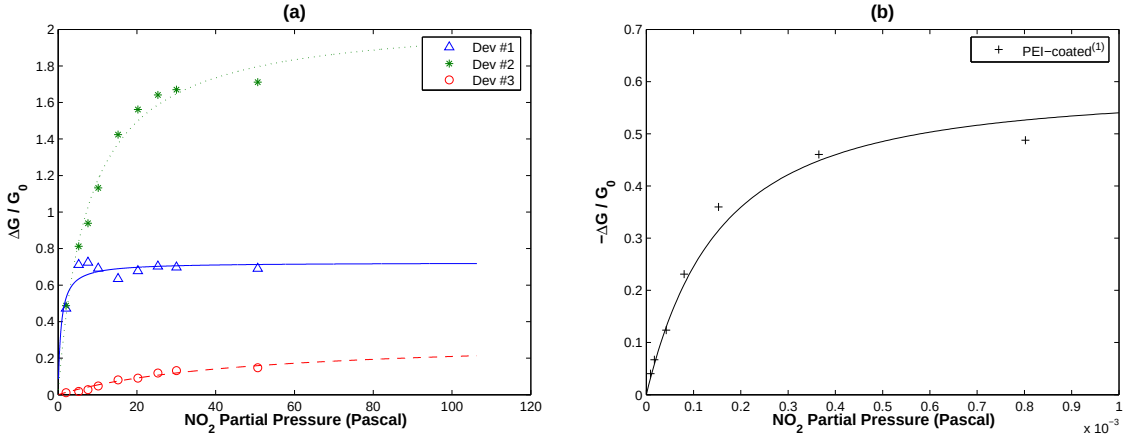

Figure 3-12: Pressure dependence of (a) standard (Cr/Au, fully-exposed) devices and (b) a PEI-coated device from [32]. Lines represent fitted curves.

Table 3.3: Extracted parameters from Langmuir constants (K_M, K_{NT}) in Table 3.2

	Fixed S=1		Fixed $E_{b.NT}$=0.8eV
	$E_{b.M}$ (eV)	$E_{b.NT}$ (eV)	S_{NT} ($\times 10^{-4}$)
Dev #1	0.53	0.53	0.256
Dev #2	0.75	0.46	0.0211
Dev #3	0.68	0.42	0.0034
Al-Dev #1	0.37	0.51	0.1122
Al-Dev #2	0.53	0.53	0.2526
CNT-exposed	-	0.49	0.0658
PEI-coated	0.60	0.74	850

Although there is no consistent interpretation of the Langmuir constants K_M and K_{NT} in Table 3.2, a few qualitative trends can be seen. First, PEI coating does indeed yield very high values, indicating either higher binding energy or sticking probability. Assuming a unity sticking coefficient (S=1), the metal-NO_2 binding energies seem to vary over a wider range, possibly indicating that gas adsorption on metal surfaces is sensitive to other factors such as surface roughness, geometry, and contact quality. Although the metal binding energies are similar or even less for Al-contacted devices, the constant b is generally higher than the standard devices. This is consistent with earlier conclusions suggesting that either binding on the metal surface plays a bigger role for Al than Cr/Au.

Theoretical calculations predict NO_2-CNT binding energies of 0.3$\sim$0.8 eV [6, 48]. Assuming a constant sticking coefficient for CNT-NO_2 binding as S_{NT}=1, the binding energies are in the range of 0.42$\sim$0.53 eV, which is fairly close to the predicted value of 0.42 eV in [6]. However, one can also assume a constant binding energy of 0.8 eV, commonly used in literature, and vary the sticking coefficient. This approximation yields sticking probabilities on the order of $\sim 10^{-5}$. Al-Dev #2 and Dev #1 are high-resistance devices dominated by semiconducting nanotubes and have a relatively high sticking probability. On the contrary, Dev #2 and #3, and Al-Dev #1 are a mixture of semiconducting and metallic CNTs, resulting in significantly lower sticking probabilities. In particular, Dev #2 and #3 are low-resistance devices where the CNT channel resistance dominates (i.e., low R_M/R_{CNT} values). This seems to indicate that the composition of metallic and semiconducting tubes might have an important role in determining the sensing response. Depending on the type of nanotube, the NO_2-CNT binding energy is known to vary [48]. The CNT channel conductance is more sensitive to NO_2 for a device composed of many nanotubes that have high binding energies than that with small binding energies. Furthermore, the effective values for the contact and CNT channel resistance also varies depending on the number and mixture of metallic and semiconducting nanotubes. Ultimately, a combination of these effects will determine whether the metal or the CNT channel dominates the sensing response.

Chapter 4

CMOS-CNT Sensor System

Exceptional electrical transport properties and nanometer scale dimensions have made CNTs promising candidates for nano-electronics. In particular, a major research thrust exists to use CNTs as interconnects or high-performance FETs. The need for such emerging technologies has become more important as conventional silicon-based CMOS technology is reaching its scaling limits. Reliability of device performance and technology integration are among the challenges towards building a CNT-based electronic system. One of the biggest hurdles is to create CNT growth procedures that are reliable and compatible with conventional CMOS processing.

While a full-scale system may not be feasible in the short term, developing hybrid systems that underlie some of the interface issues is an important step towards integration. Such effort has lead to the development of a CMOS-CNT sensor system. Designing a CNT-based sensor system has its own merits in addition to creating a complete system with a backend circuitry. The CNT sensors fabricated in this work are simple resistive devices in a FET structure, and thus highlights the need of interfacing to a CNT FET array with a wide device variations. Although reducing such variations is important in terms of reliability, the limits of such improvement is unclear and increasing variability is a trend already seen in CMOS processing: as characteristic length scales are shrinking and die sizes increase, design considerations for variation-tolerant circuits is becoming increasingly important [43].

In this chapter, a brief summary of the collaborative effort with Taeg Sang Cho

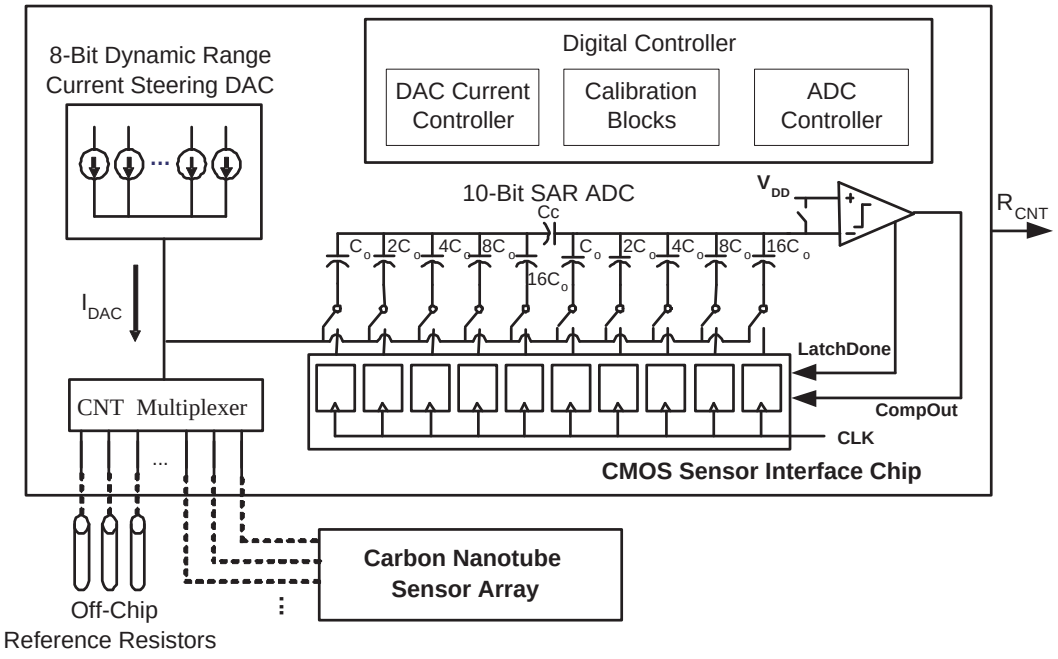

Figure 4-1: Diagram of CMOS sensor interface. Courtesy of Taeg Sang Cho [8]

at MIT is presented. Details of the circuit design and analysis can be found in [8]. Figure 4-1 shows the schematic diagram of Cho's circuit architecture.

The main purpose of the digital controller is two-fold: to control the initial calibration of the resistance of each CNT device, and to adjust various sub-block during the data sampling sequence. After the calibration stage, the resistance of each CNT device is measured in turn, and this loop continues indefinitely. The resistance for each device is measured by sourcing a constant current through the CNT FET and measuring the voltage level by an analog-digital-converter (ADC). Recall that the resistance can vary over 3∼4 orders of magnitude. The chip employs several current sources set at various current levels. Due to the wide dynamic range in resistance values, the current source dynamically self-adjusts to the right range that gives the optimal range of output voltage at the right bit-resolution. The chip then continually streams the 20-bit resistance values as an output. This CMOS circuit was fabricated by National Semiconductors using 0.18μm technology, and was designed to meet requirements for low energy consumption, wide dynamic range of CNT resistance, and high bit-resolution for resistance monitoring.

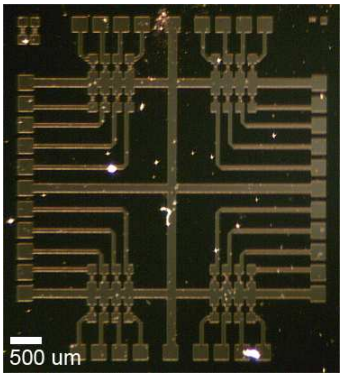

Figure 4-2: Die photo of CNT sensor array. Metal pads are designed to be placed along the outer boundary, which is optimal for wire-bonding.

Cho's circuit interfaces to an array of 32 CNT sensor devices. Unlike the devices used in Chapters 2 and 3, a smaller 8×4 array is used for the sensor system. The metal pads are also optimally designed for wire bonding. Figure 4-2 shows the new die photo of the CNT sensor array. The fabrication procedures are identical to that presented in Section 2.1 except that the substrate has an oxide thickness of 100 nm.

Experimental procedures are similar to that described in Section 2.3.1. The major difference is that the gas chamber is bigger in order to accommodate the chip holder and electrical wires, and that the measurement setup is replaced by Cho's CMOS chip. Cho's circuit directly interfaces to the CNT sensor chip through electrical wires. A logic analyzer was used generate the appropriate input signals to the chip and collect the 20-bit resistance values for each CNT device. Figure 4-3 shows the gas chamber and the circuit boards that connect the CNT sensor array and the CMOS interface. Ultimately, a single-chip solution is desirable for achieving true system integration. Meitl et al. present a stamp-based method that reliably transfers microstructure from one substrate to another. Using such methods to seamlessly integrate CMOS processing CNT growth procedures is an area of future work.

Two sensor chips were exposed to various concentrations of NO_2. Figure 4-4 shows the transient resistance measurements from the system, and thus confirms successful gas detection of the CMOS-CNT sensor system. Initial resistance values of devices shown in Figure 4-4 range from 18kΩ to 1.4MΩ.

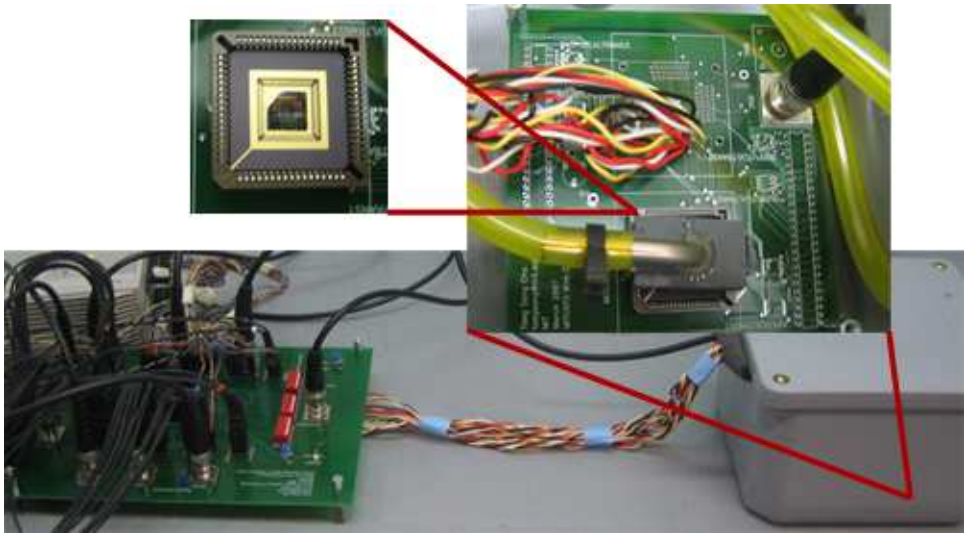

Figure 4-3: Experimental setup for CMOS-CNT system testing. CNT sensor chip is placed on a chip holder inside the gas chamber. CMOS chip placed outside of the chamber. Gas lines, power sources, and logic analyzer are not shown. Courtesy of Taeg Sang Cho

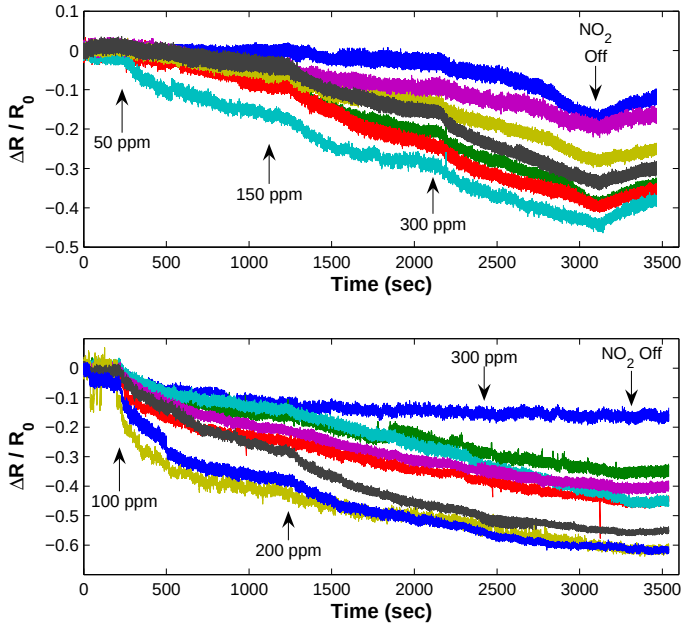

Figure 4-4: Measurement results from CMOS-CNT system. Two different sensor chips were exposed to NO_2 at different concentrations.

Chapter 5

Conclusions

In this thesis, CNT FET arrays were characterized, connecting the underlying physics of gas adsorption to the electrical response of a CNT sensor device. Each array was exposed to varying concentrations of NO_2 in a constant stream of Ar. The amount of resistance change for a device at a given concentration was measured to be roughly linear as a function of its initial resistance. This relation was further modeled by treating gas adsorption on the metal contact and CNT as two separate processes. The contact resistance is affected by gas adsorption due to SB modulation, and the CNT channel resistance is affected by charge transfer or DOS modification. A Langmuir isotherm was used to link the physics of the gas adsorption process to a macroscopic conductance model. The exponential dependence of current on the SB height was explicitly added in, which is commonly left out. Depending on the gas molecule, the relative binding energy to the metal vs. CNT surfaces, charge transfer along the CNT, and polarizability of the gas molecule will determine the time constant (response) and amount of conductance change.

Transient traces of Al and Cr/Au contacted devices showed that the model fit very well to the measured data. Al-contacted devices generally resulted in a much higher initial resistance value, but showed a faster transient response and stronger metal-NO_2 binding. This result, along with the ΔG vs. G_0 curve of an entire array indicated that the NO_2 sensing response is dominated by the metal. Partially-exposed devices (through a PMMA layer) were fabricated to further understand this effect. CNT-

exposed devices still showed responses similar to the fully-exposed devices, while the metal-exposed devices did not seem to respond, except by NO_2 diffusing through the PMMA layer. These results suggest that CNT-NO_2 interaction is still important, and other surface interactions right at the metal-CNT junction may play an important role. Examining $\Delta G/G_0$ as a function of the NO_2 partial pressure indicated that the mixture of semiconducting and metallic devices might also affect the magnitudes of the effective contact and channel resistance, and thus ultimately the extent to which effect dominates the sensor response.

Finally, a simple prototype CMOS-CNT sensor system was demonstrated in Chapter 4. The CMOS interface was designed by T.S. Cho, and presents an important solution for addressing the need for reliable and variation-tolerant circuit architectures when integrating conventional CMOS and new nano-materials. Ultimately, the ability to functionalize the CNTs for detecting specific gas species, and seamlessly integrate CMOS and CNT fabrication procedures, will determine the usefulness of full scale CNT sensing applications. Understanding the effects of CNT defects, choice of metal contact and geometry, and non-uniform surface coverage are important areas of future work that will further elucidate the effects on the metal and CNT channel upon gas adsorption.

Bibliography

[1] Jan Andzelm, Niranjan Govind, and Amitesh Maiti. Nanotube-based gas sensors - role of structural defects. *Chem. Phys. Lett.*, 421(1-3):58 – 62, 2006.

[2] Phaedon Avouris, Joerg Appenzeller, Richard Martel, and Shalom J. Wind. Carbon nanotube electronics. *Proc. of the IEEE*, 91(11):1772 – 1783, 2003.

[3] Keith Bradley, Jean-Christophe P. Gabriel, Mikhail Briman, Alexander Star, and George Grüner. Charge transfer from ammonia physisorbed on nanotubes. *Phys. Rev. Lett.*, 91(21):218301, Nov 2003.

[4] Keith Bradley, Jean-Christophe P. Gabriel, Alexander Star, and George Gruner. Short-channel effects in contact-passivated nanotube chemical sensors. *Appl. Phys. Lett.*, 83(18):3821 – 3823, 2003.

[5] N. Chakrapani, Y.M. Zhang, S.K. Nayak, J.A. Moore, D.L. Carroll, Y.Y. Choi, and P.M. Ajayan. Chemisorption of acetone on carbon nanotubes. *J. Phys. Chem. B*, 107(35):9308–9311, 2003.

[6] H. Chang, Jae Do Lee, Seung Mi Lee, and Young Hee Lee. Adsorption of nh_3 and no_2 molecules on carbon nanotubes. *Appl. Phys. Lett.*, 79(23):3863 –, 2001.

[7] Z. Chen, J. Appenzeller, J. Knoch, Y.-M. Lin, and Ph. Avouris. The role of metal-nanotube contact in the performance of carbon nanotube field-effect transistors. *Nano Lett.*, 5(7):1497–1502, 2005.

[8] Taeg Sang Cho. An energy efficient cmos sensor interface to carbon nanotube sensor arrays. Master's thesis, Massachusetts Institute of Technology, Department of Electrical Engineering and Computer Science, 2007.

[9] Philip G. Collins, Keith Bradley, Masa Ishigami, and A. Zettl. Extreme Oxygen Sensitivity of Electronic Properties of Carbon Nanotubes. *Science*, 287(5459):1801–1804, 2000.

[10] X. Cui, M. Freitag, R. Martel, L. Brus, and P. Avouris. Controlling energy-level alignments at carbon nanotube/au contacts. *Nano Lett.*, 3(6):783–787, 2003.

[11] M. Grujicic, G. Cao, and R. Singh. The effect of topological defects and oxygen adsorption on the electronic transport properties of single-walled carbon-nanotubes. *Appl. Surf. Sci.*, 211(1-4):166 – 83, 2003.

[12] S. Heinze, J. Tersoff, R. Martel, V. Derycke, J. Appenzeller, and Ph. Avouris. Carbon nanotubes as schottky barrier transistors. *Phys. Rev. Lett.*, 89(10):106801, Aug 2002.

[13] C. Huckstadt, S. Schmidt, S. Hufner, F. Forster, F. Reinert, and M. Springborg. Work function studies of rare-gas/noble metal adsorption systems using a kelvin probe. *Phys. Rev. B*, 73(7):75409 – 1, 2006/02/15.

[14] S. Iijima. Helical microtubules of graphitic carbon. *Nature*, 354(6348):56 –, 1991.

[15] A. Javey, R. Tu, D.B. Farmer, J. Guo, R.G. Gordon, and H. Dai. High performance n-type carbon nanotube field-effect transistors with chemically doped contacts. *Nano Lett.*, 5(2):345–348, 2005.

[16] Ali Javey, Jing Guo, Qian Wang, Mark Lundstrom, and Hongjie Dai. Ballistic carbon nanotube field-effect transistors. *Nature*, 424(6949):654 – 657, 2003.

[17] Woong Kim, Ali Javey, Ryan Tu, Jien Cao, Qian Wang, and Hongjie Dai. Electrical contacts to carbon nanotubes down to 1 nm in diameter. *Appl. Phys. Lett.*, 87(17):173101 – 173103, 2005.

[18] J. Kong and H. Dai. Full and modulated chemical gating of individual carbon nanotubes by organic amine compounds. *J. Phys. Chem. B*, 105(15):2890–2893, 2001.

[19] Jing Kong, Nathan R. Franklin, Chongwu Zhou, Michael G. Chapline, Shu Peng, Kyeongjae Cho, and Hongjie Dai. Nanotube Molecular Wires as Chemical Sensors. *Science*, 287(5453):622–625, 2000.

[20] Jing Kong, Hyongsok T. Soh, Alan M. Cassell, Calvin F. Quate, and Hongjie Dai. Synthesis of individual single-walled carbon nanotubes on patterned silicon wafers. *Nature*, 395(6705):878 – 881, 1998.

[21] C.Y. Lee, S. Baik, J. Zhang, R.I. Masel, and M.S. Strano. Charge transfer from metallic single-walled carbon nanotube sensor arrays. *J. Phys. Chem. B*, 110(23):11055–11061, 2006.

[22] C.Y. Lee and M.S. Strano. Understanding the dynamics of signal transduction for adsorption of gases and vapors on carbon nanotube sensors. *Langmuir*, 21(11):5192–5196, 2005.

[23] Fran çois Léonard and A. Alec Talin. Size-dependent effects on electrical contacts to nanotubes and nanowires. *Phys. Rev. Lett.*, 97(2):026804 –, 2006.

[24] Fran çois Léonard and J. Tersoff. Novel length scales in nanotube devices. *Phys. Rev. Lett.*, 83(24):5174–5177, Dec 1999.

[25] Fran çois Léonard and J. Tersoff. Role of fermi-level pinning in nanotube schottky diodes. *Phys. Rev. Lett.*, 84(20):4693–4696, May 2000.

[26] Xiaolei Liu, Zhicheng Luo, Song Han, Tao Tang, Daihua Zhang, and Chongwu Zhou. Band engineering of carbon nanotube field-effect transistors via selected area chemical gating. *Appl. Phys. Lett.*, 86(24):243501 –, 2005.

[27] R.Q. Long and R.T. Yang. Carbon nanotubes as a superior sorbent for nitrogen oxides. *Industrial & Engineering Chemistry Research*, 40(20):4288–4291, 2001.

[28] P.L. McEuen, M.S. Fuhrer, and Hongkun Park. Single-walled carbon nanotube electronics. *IEEE Trans. on Nanotechnology*, 1(1):78 – 85, 2002.

[29] J. A. Misewich, R. Martel, Ph. Avouris, J. C. Tsang, S. Heinze, and J. Tersoff. Electrically Induced Optical Emission from a Carbon Nanotube FET. *Science*, 300(5620):783–786, 2003.

[30] Shu Peng and Kyeongjae Cho. Chemical control of nanotube electronics. *Nanotechnology*, 11(2):57–60, 2000.

[31] J.D. Plummer, M.D. Deal, and P.B. Griffin. *Silicon VLSI Technology: Fundamentals Practice and Modeling*. Prentice Hall, 2000.

[32] P. Qi, O. Vermesh, M. Grecu, A. Javey, Q. Wang, H. Dai, S. Peng, and K.J. Cho. Toward large arrays of multiplex functionalized carbon nanotube sensors for highly sensitive and selective molecular detection. *Nano Lett.*, 3(3):347–351, 2003.

[33] M.W. Roberts and C.S. McKee. *Chemistry of the Metal-Gas Interface*. Monographs on the Physics and Chemistry of Materials. Oxford University Press, 10 January 1978.

[34] J.A. Robinson, E.S. Snow, S.C. Badescu, T.L. Reinecke, and F.K. Perkins. Role of defects in single-walled carbon nanotube chemical sensors. *Nano Lett.*, 6(8):1747–1751, 2006.

[35] S. Santucci, S. Picozzi, F. Di Gregorio, L. Lozzi, C. Cantalini, L. Valentini, J.M. Kenny, and B. Delley. No_2 and co gas adsorption on carbon nanotubes: experiment and theory. *J. Chem. Phys.*, 119(20):10904 – 10, 2003/11/22.

[36] M. Shim, N.W. Shi Kam, R.J. Chen, Y. Li, and H. Dai. Functionalization of carbon nanotubes for biocompatibility and biomolecular recognition. *Nano Lett.*, 2(4):285–288, 2002.

[37] E. S. Snow, F. K. Perkins, E. J. Houser, S. C. Badescu, and T. L. Reinecke. Chemical Detection with a Single-Walled Carbon Nanotube Capacitor. *Science*, 307(5717):1942–1945, 2005.

[38] E.S. Snow, J.P. Novak, P.M. Campbell, and D. Park. Random networks of carbon nanotubes as an electronic material. *Appl. Phys. Lett.*, 82(13):2145 – 2147, 2003.

[39] E.S. Snow and F.K. Perkins. Capacitance and conductance of single-walled carbon nanotubes in the presence of chemical vapors. *Nano Lett.*, 5(12):2414–2417, 2005.

[40] T. Someya, J. Small, P. Kim, C. Nuckolls, and J.T. Yardley. Alcohol vapor sensors based on single-walled carbon nanotube field effect transistors. *Nano Lett.*, 3(7):877–881, 2003.

[41] G.A. Somorjai. *Intro. to Surface Chemistry and Catalysis*. Wiley-Interscience, 1994.

[42] J. Suehiro, H. Imakiire, S. Hidaka, Weidong Ding, Guangbin Zhou, K. Imasaka, and M. Hara. Schottky-type response of carbon nanotube no_2 gas sensor fabricated onto aluminum electrodes by dielectrophoresis. *Sens. Actuators B, Chem.*, 114(2):943 – 9, 2006/04/26.

[43] J. Tschanz, K. Bowman, and V. De. Variation-tolerant circuits: circuit solutions and techniques. *Design Automation Conference, 2005. Proc. 42nd*, pages 762–73, 2005.

[44] L. Valentini, F. Mercuri, I. Armentano, C. Cantalini, S. Picozzi, L. Lozzi, S. Santucci, A. Sgamellotti, and J.M. Kenny. Role of defects on the gas sensing properties of carbon nanotubes thin films: experiment and theory. *Chem. Phys. Lett.*, 387(4-6):356 – 61, 2004.

[45] H.-S.P. Wong, J. Appenzeller, V. Derycke, R. Martel, S. Wind, and Ph. Avouris. Carbon nanotube field effect transistors - fabrication, device physics, and cir-

cuit implications. *Digest of Technical Papers - IEEE International Solid-State Circuits Conference*, pages 367 – 370, 2003.

[46] A. Zangwill. *Physics at Surfaces*. Cambridge University Press, 2001.

[47] Jian Zhang, A. Boyd, A. Tselev, M. Paranjape, and P. Barbara. Mechanism of no_2 detection in carbon nanotube field effect transistor chemical sensors. *Appl. Phys. Lett.*, 88(12):123112 – 1, 2006/03/20.

[48] Jijun Zhao, Alper Buldum, Jie Han, and Jian Ping Lu. Gas molecule adsorption in carbon nanotubes and nanotube bundles. *Nanotechnology*, 13(2):195 – 200, 2002.

[49] Jijun Zhao, Alper Buldum, Jie Han, and Jian Ping Lu. Gas molecule adsorption in carbon nanotubes and nanotube bundles. *Nanotechnology*, 13(2):195–200, 2002.